Applied Catalysis B: Environmental 276 (2020) 119102

Contents lists available at ScienceDirect

Applied Catalysis B: Environmental

journal homepage: www.elsevier.com/locate/apcatb

Efficient CO_2 conversion to formic acid in a novel microbial photoelectrochemical cell using a visible-light responsive Co_3O_4 nanorod-arrayed photocathode

Jing Wu[a], Xiaoyu Han[a], Da Li[a,*], B.E. Logan[b], Jia Liu[a], Zhaohan Zhang[a], Yujie Feng[a,*]

[a] State Key Laboratory of Urban Water Resource and Environment, School of Environment, Harbin Institute of Technology. No 73 Huanghe Road, Nangang District, Harbin 150090, China

[b] Department of Civil and Environmental Engineering, Penn State University, 212 Sackett Building, University Park, PA, 16802, USA

ARTICLE INFO

Keywords:
Microbial photoelectrochemical cell
Co_3O_4nanorod-arrayed photocathode
Bioenergy
CO_2conversion
Synergistic effect

ABSTRACT

A microbial photoelectrochemical cell (MPEC) is a self-biased, solar-driven device combining bioenergy with solar energy to produce sustainable electricity and chemicals. Here, an MPEC with a p-type Co_3O_4 nanorod-arrayed photocathode and bio-anode was constructed that matched well the redox potentials of anode microorganisms with the band gap of the Co_3O_4. The yield of formic acid produced by this MPEC under visible light irradiation with an external resistance of 300 Ω was 239 ± 10 μmol in 10 h, which was 1.8 times that produced by a bare Co_3O_4 photocathode under visible light, and 4.9 times that produced by the MPEC operated in dark. The maximum power density was 331 ± 4 mW m^{-2} under visible light, compared to 175 ± 25 mW m^{-2} in the dark. This study of MPEC with the synergistic effect of light energy and bioenergy opens up new opportunities for applications in environmental treatment of wastewaters and chemicals production.

1. Introduction

The combustion of fossil fuels has led to excessive emissions of CO_2 into the atmosphere, resulting in climate change which is a great threat to the goal of sustainable development [1–3]. Conversion of CO_2 to chemical fuels is a potential way for producing chemicals and reducing CO_2 emissions [4–6]. In general, photocatalysis [7–9], electrocatalysis [10–12] and photoelectrochemical catalysis [13–15] are three commonly used methods for CO_2 conversion in water. Compared with single photocatalytic or electrocatalytic systems, photoelectrocatalytic CO_2 conversion exhibits more advantages: the assistance of light energy could lower the input electricity in comparison with electrocatalytic CO_2 conversion; the applied external voltage could enhance the photocatalytic charge separation and efficiency of photoelectrode compared with photocatalytic process [16–18]. In a photoelectrocatalytic CO_2 conversion process, a photoelectrode with excellent photocatalytic and electrocatalytic properties is of great importance [19]. Among kinds of semiconductor materials, Co_3O_4, as a p-type, visible-light responsive photocatalysis, with remarkable electrochemical performance [20–22], is regarded as one of the most promising candidates to serve as the photoelectrode that could efficiently realize the photoelectrocatalytic CO_2 conversion. Recent studies has demonstrated that Co_3O_4 has the ability to reduce CO_2 into value-added chemical fuels in the photoelectrocatalytic process [23–25]. Although the photoelectrocatalytic CO_2 conversion shows more advantages, the input of additional electrical energy increases the cost and cannot satisfy the requirement for industrial applications.

A microbial fuel cell (MFC) is a bioelectrochemical system that provides an efficient way to oxidize organic matter in wastewaters using electrochemically active microorganisms to remove pollutants and produce electricity at the same time [26–28]. Recently, an MFC with a light-driven semiconductor photocathode (MPEC) was developed that could generate hydrogen gas by combining the energy from the microbial degradation of organic matter with solar energy. Electricity derived from the degradation of organic matter by microorganisms on the anode is used in the MPEC to supply electrons to the photocathode, enhancing charge separation of semiconductor photocatalysis and improving photocatalytic efficiency. A visible-light driven MPEC with a Cu_2O nanowire photocathode was constructed by Qian et al. [29], and substantial current generation was successfully obtained in this MPEC at zero bias by coupling bioenergy produced by the anode with light on the cathode. An MPEC with a CuO nanowire-arrayed photocathode was also fabricated by Sun et al. [30], and a maximum power density of 46 mW m^{-2} under light irradiation was generated,

* Corresponding authors.
E-mail addresses: lidacumt@163.com (D. Li), yujief@hit.edu.cn (Y. Feng).

https://doi.org/10.1016/j.apcatb.2020.119102
Received 8 December 2019; Received in revised form 4 May 2020; Accepted 5 May 2020
Available online 11 May 2020
0926-3373/

which was 1.26 times that generated in the dark. Subsequently, an MPEC with a composite Cu_2O/NiO_x photocathode for efficient H_2 production was constructed by Liang et al. [31], and a H_2 production rate of 5 μL h^{-1} cm^{-2} was obtained under continuous light illumination with 0.2 V external bias. However, the visible-light driven copper oxide photocathodes used in these studies were unstable, and most constructed MPECs have been used for H_2 production. There have not yet been any studies on CO_2 conversion to chemicals in the photocathode chamber of an MPEC.

Here, an MPEC was constructed that used a Co_3O_4 nanorod-arrayed photocathode for CO_2 conversion to formic acid by co-utilization of light energy and bioenergy. Using electrons derived from the anodic conversion of biodegradable organic matter, the Co_3O_4 nanorod-arrayed photocathode exhibited enhanced photocatalytic activity for CO_2 conversion compared with the control (Co_3O_4 nanorod-arrayed photocatalyst alone) under visible light irradiation. The COD removal efficiency, coulombic efficiency and power density of this MPEC were also examined for the MPEC compared to controls.

2. Experimental methods

2.1. Reagents

The chemical reagents included cobalt chloride hexahydrate ($CoCl_2{\cdot}6H_2O$), urea ($CO(NH_2)_2$), nickel foam, sodium sulfate (Na_2SO_4), sodium acetate (CH_3COONa), ammonium chloride (NH_4Cl), potassium chloride (KCl), sodium dihydrogen phosphate ($NaH_2PO_4{\cdot}2H_2O$), disodium hydrogen phosphate ($Na_2HPO_4{\cdot}12H_2O$), vitamins and trace minerals. All the reagents were used as received without further purification. Deionized water was used throughout this study.

2.2. Preparation of Co_3O_4 nanorod-arrayed photocathode

To prepare the Co_3O_4 nanorod-arrayed photocathode, nickel foam was washed with ultrasonication in acetone and ethanol for 20 min. Then, $CoCl_2{\cdot}6H_2O$ (0.95 g) and $CO(NH_2)_2$ (1.20 g) were put into a Teflon-lined stainless steel chamber with 50 mL of deionized water. The mixture was stirred for 0.5 h, and then the pretreated nickel foam was vertically placed into the container, and then sealed and kept at 95 °C for 8 h in an oil bath pan with continuous stirring. After cooling to room temperature, the nickel foam was rinsed with deionized water with ultrasonication for 3 min, dried at 60 °C for 6 h, and then annealed at 250 °C for 1 h, producing the final Co_3O_4 nanorod-arrayed photocathode.

2.3. Reactor setup and operation

2.3.1. Bio-anode culture

The bio-anode was cultivated in a single-chamber air-cathode microbial fuel cell (MFC) configuration with a volume of 56 mL (diameter of 3 cm, 8 cm long) (**Fig. S1**). The anode was a carbon fiber brush which was 7 cm long and 3 cm in diameter. The carbon brush was first cleaned by soaking in pure acetone for 12 h, and then heated in a muffle furnace at 450 °C for 0.5 h. The chamber was inoculated with municipal wastewater and a medium containing sodium acetate (1.0 g/L), 50 mM phosphate buffer solution (0.13 g/L of KCl, 0.31 g of NH_4Cl, 3.32 g/L of $NaH_2PO_4{\cdot}2H_2O$ and 10.32 g/L of $Na_2HPO_4{\cdot}12H_2O$, 12.5 mL of a trace mineral solution, and 5 mL of a vitamin solution. The air cathode was made by the rolling press method [32]. The external resistance of the MFC was kept at 1000 Ω during acclimation. The chamber were kept anaerobic except when the inoculation medium was refilled every 24 h. The bio-anode was acclimated for approximately 3 weeks until the carbon fiber brush was enriched with electrochemically active microorganisms as shown by a stable output voltage of ~500 mV (**Fig. S2**). All tests were conducted at a constant temperature of 30 °C, and repeated three times.

2.3.2. MPEC construction and operation

The acclimated bio-anode was transferred into the MPEC containing a Co_3O_4 nanorod-arrayed photocathode in an H-type, two-chamber reactor (**Fig.** S3). The anode and photocathode chambers each had a volume of 100 mL, with the two chambers separated by proton exchange membrane (PEM, 2.3 cm^2; Beijing Anketech Membrane Separation Engineering & Technology Co., Ltd., China) held in a tube with an inner diameter of 1.7 cm and a length of 1.2 cm on each side of the membrane. The anode was inserted vertically into the anode chamber through the small hole in the PTFE cover. The cathode (projected area of 3.8 cm^2) was held using an electrode clamp, and inserted vertically into the cathode chamber through the small hole on the PTFE cover. A quartz window was set on the photocathode chamber for transmission of light. The photocatalytic cathode and microbial anode were connected with wires across an external resistance. The light source was a 150 W xenon lamp (GY-10A, Tuopu Co. Ltd., China, 380 − 780 nm). Na_2SO_4 (0.1 M) was used as supporting electrolyte in the photocathode chamber.

2.4. Photocathode characterization

X-ray diffraction (XRD) patterns were obtained using a Rigaku D/MAX III-3B diffractometer with Cu Kα source (40 kV and 30 mA) to investigate the crystal phase structure and composition of photocathode. Ultraviolet-vis diffuse reflectance spectroscopy (UV–vis DRS) was conducted using a Shimadzu UV-2550 spectrophotometer equipped with an integrating sphere detector, with $BaSO_4$ as the reflectance sample. The surface morphology was obtained using a field-emission scanning electron microscope (SEM, FEI Quanta 200 F). Transmission electron microscopy (TEM) was obtained using a JEM-3010 electron microscope (JEOL, Japan). X-ray photoelectron spectroscopy was conducted using a PHI-5700 ESCA instrument with Al Kα radiation. N_2 adsorption/desorption was tested by Brunauer-Emmett-Teller (BET) with a 3H-2000PS1 surface area analyzer (Beishide, China) at 77 K.

2.5. Photoelectrochemical measurements of the photocathode

Linear sweep voltammetry (LSV) curves and electrochemical impedance spectra (EIS) of the photocathode were measured in a three-electrode system with an electrochemical workstation (Princeton Applied Research, Versa STAT3). The electrolyte was a Na_2SO_4 solution (0.1 M). The nanorod-arrayed Co_3O_4 was used as a working electrode, Pt foil (99.9 %) as a counter electrode, and a saturated calomel electrode (SCE, +0.242 V vs standard hydrogen electrode; SHE) as the reference electrode. The frequency of EIS test was set from 0.01 Hz to 100,000 Hz, with an amplitude of 10 mV (RMS). The light source was a 150 W xenon (GY-10A, Tuopu Co. Ltd., China, 380 − 780 nm).

2.6. Data collection and analysis of MPEC system

The output voltages (U) of the MPEC system were recorded with a data acquisition board (PISO-813, ICP DAS CO., Ltd.). The polarization curves and power density of MPEC under light and dark conditions were obtained by varying the external resistance over a range from 10,000 to 100 Ω. A multimeter was used to record the cell voltage, anode and cathode potentials. The current density was obtained with the formula of $I = U/RA$, where U is the cell voltage, R the external resistance, and A the projected surface area of the cathode. The measured anode and cathode potentials, power density were corrected for ohmic drops between the working and reference electrodes, and calculated as previously reported [33,34].

2.7. CO_2 conversion in MPEC

CO_2 conversion using the single Co_3O_4 nanorod-arrayed photocathode with light irradiation was first examined in a single

photocathode chamber. Prior to CO_2 conversion tests, high purity CO_2 gas was sparged into the Na_2SO_4 electrolyte (0.1 M, 70 mL) for 0.5 h at a gas flowrate of 20 mL min^{-1} to remove the residual air. For conversion tests, the gas flowrate of CO_2 was maintained at 10 mL min^{-1}. The light source was same as that used in the photoelectrochemical measurements of photocathode. During irradiation, 1.5 mL of liquid was taken from the cathode chamber every 1 h over the duration of the experiment (10 h) to evaluate chemical production. CO_2 conversion tests were also conducted using only the single Co_3O_4 nanorod-arrayed photocathode without light irradiation.

CO_2 conversion performance of the MPEC system was also tested with and without light irradiation. For light irradiation tests, the reactor was first kept in an open-circuit state and saturated calomel electrodes (SCE, +0.242 V vs standard hydrogen electrode; SHE) were placed into the cathode and anode chambers to monitor the electrode potentials. Before these experiments, high purity CO_2 gas was sparged into the cathode Na_2SO_4 electrolyte (0.1 M, 70 mL) at 20 mL min^{-1}, and the anode chamber was replaced with fresh medium. When the anode potential reached about −500 mV, the cathode and anode were connected with wires across a 300 Ω resistor. After the xenon light was turned on, the gas flowrate of CO_2 in cathode was reduced to 10 mL min^{-1} and samples were taken of the catholyte as described above. The anode and cathode potentials, and the voltages were recorded using a data acquisition system.

The products of CO_2 conversion were analyzed using an ion chromatograph (IC 6100, Wanyi, AnHui, China). Before analysis, the liquid samples were diluted 10 times and filtered through a 0.22 μm pore diameter syringe filter. The process of CO_2 conversion using this MPEC without light irradiation was the same as the process of CO_2 conversion with light irradiation except for the omission of the light.

The concentration of acetate in the anolyte at the beginning and end of the tests was based on its chemical oxygen demand (COD). The COD removal rate and coulombic efficiency (CE) were calculated as previously reported based on the changes in COD and the measured current [35].

3. Results and discussion

3.1. Characterization of photocathode

The XRD patterns of the Co_3O_4 nanorod-arrayed powder removed from the Ni foam substrate showed that all the diffraction peaks were derived from Co_3O_4. The peaks and the corresponding crystal planes of the spinel Co_3O_4 phases were at 19.0 (111), 31.2 (220), 36.8 (311), 44.8 (400), 59.4 (511) and 65.2° (440) (JCPDS 09−0418) (Fig. 1A), and no other peaks of impurities were observed. The UV diffraction reflection spectroscopy of the Co_3O_4 nanorod-arrayed photocathode showed obvious optical absorption in both the ultraviolet and visible light wavelengths (Fig. 1B). To calculate the band gap values, the plot of $(Ah\nu)^2$ vs $h\nu$ was investigated, where A is the absorption and $h\nu$ is the photon energy (Fig. 1B, **inset**). A band gap of 1.43 eV calculated from the plot was attributed to the transition from O^{2-} to Co^{3+}. Another calculated band gap of 2.39 eV was attributed to the transition of O^{2-} to Co^{2+}, which was the "true" energy gap corresponding to inter-band transitions [36]. The results of the calculated band gaps demonstrated that the synthetic Co_3O_4 nanorod-arrayed photocathode could absorb visible light and was a visible light responsive photocatalyst. The conduction band and valence band potentials of this Co_3O_4 photocathode were further calculated with :

$$E_{VB} = X - E^e + 0.5Eg \quad (1)$$

$$E_{CB} = E_{VB} - Eg \quad (2)$$

where E_{VB} and E_{CB} are the potentials of conduction band edge and valence band edge, respectively, X and Eg are the electronegativity and band gap of a semiconductor, respectively, and E^e is the energy of free electrons vs. hydrogen (about 4.5 eV/NHE) [37]. The X values of Co_3O_4 is 5.93 eV [38,39]. Thus, the E_{VB} and E_{CB} of Co_3O_4 were calculated to be 2.625 eV and 0.235 eV (vs. NHE).

The XPS spectra showed large peaks corresponding to Co and O. Two major peaks were observed with a spin-energy separation of 15 eV in the Co 2p spectra (Fig. 1C). The peak at the binding energy of 779.84 eV corresponded to Co 2p3/2, and a peak at 794.84 eV was to that expected for Co 2p1/2, which were characteristics of the Co_3O_4 phase [40]. In the O 1s spectra (Fig. 1D), the observed peaks at about 531.7 eV and 530.1 eV were derived from the lattice oxygen atom in Co_3O_4 and the −OH species adsorbed on the surface of Co_3O_4 [41,42].

The SEM image of the Co_3O_4 photocathode showed a high density of Co_3O_4 nanorods and were grown uniformly on the Ni foam substrate (Fig. 2A and B). The Co_3O_4 nanorod arrays grew almost vertically on the Ni foam substrate (Fig. 2C). The TEM image (Fig. 2D) of a single Co_3O_4 nanorod scraped off the Ni substrate showed that the diameter of a Co_3O_4 nanorod was around 80 nm, and that there were many mesopores distributed on the surface. The lattice spacing of 0.47 nm in the HRTEM image (Fig. 2E) corresponded to the (111) crystal planes of spinel Co_3O_4 [43], consistent with the XRD data. The corresponding SAED pattern (Fig. 2F) demonstrated that the Co_3O_4 nanorod had a polycrystalline structure. [44]

N_2 adsorption-desorption isotherm and corresponding Barrett–Joyner–Halenda (BJH) pore size distributions were obtained to further investigate the structure of the mesopores (Fig. 3). The pores of the mesoporous structures were 12.0 nm. Moreover, the Co_3O_4 nanorod exhibited a BET surface area of 40.7 $m^2 g^{-1}$ and pore volume of 0.2 $cm^3 g^{-1}$. These structural characteristics would benefit the adsorption of CO_2 on the surface of the Co_3O_4 nanorod-arrayed photocathode during the CO_2 conversion process.

3.2. Photoelectrochemical performance of photocathode

The linear sweep voltammetry (LSV) curves of the Co_3O_4 nanorod-arrayed photocathode in 0.1 M N_2 or CO_2 saturated Na_2SO_4 aqueous solution were performed under visible light irradiation and in the dark (Fig. 4A). In the N_2-saturated electrolyte, the current density curves of Co_3O_4 photoelectrode were relatively flat whether under irradiation or not. However, a dramatic enhancement in current density with regard to CO_2 reduction in CO_2-saturated electrolyte was observed under both irradiation and in dark. The onset potential of this Co_3O_4 photocathode observed in dark was approximately -0.85 V, which was more positive than that of a hierarchical Co_3O_4 electrode reported previously [24], indicating that the Co_3O_4 photocathode had a superior electrocatalytic capability for CO_2 reduction. The onset potential moved to a more positive value and the reduction current density was obviously larger with light irradiation than that in dark, confirming a faster CO_2 reduction rate due to the generation of the photogenerated electron-hole pairs under visible light irradiation. The EIS spectra of the Co_3O_4 photocathode were analyzed using an equivalent circuit model (Fig. 4B), where R_s is the resistance of the electrolyte between two electrodes, C_{dl} the double layer capacitance, R_{ct} the charge transfer resistance, and W the Warburg impedance [9]. The charge transfer resistance was R_{ct} = 0.013 Ω in the light, compared to 0.28 Ω in the dark (**Table S1**). The decreased charge transfer resistance in the light indicated that the Co_3O_4 photocathode had a better electron transfer ability with light irradiation. The photoelectrochemical performance thus confirmed that the p-type Co_3O_4 could function as an efficient photocathode for effective photoelectrocatalytic CO_2 reduction.

3.3. Evaluation of MPEC performance

The current densities produced by the MPEC were examined with and without visible light irradiation. With an external resistance of 300 Ω, the generated current density in dark was 21.6 μA cm^{-2}, which gradually increased to 60.2 μA cm^{-2} under visible light irradiation

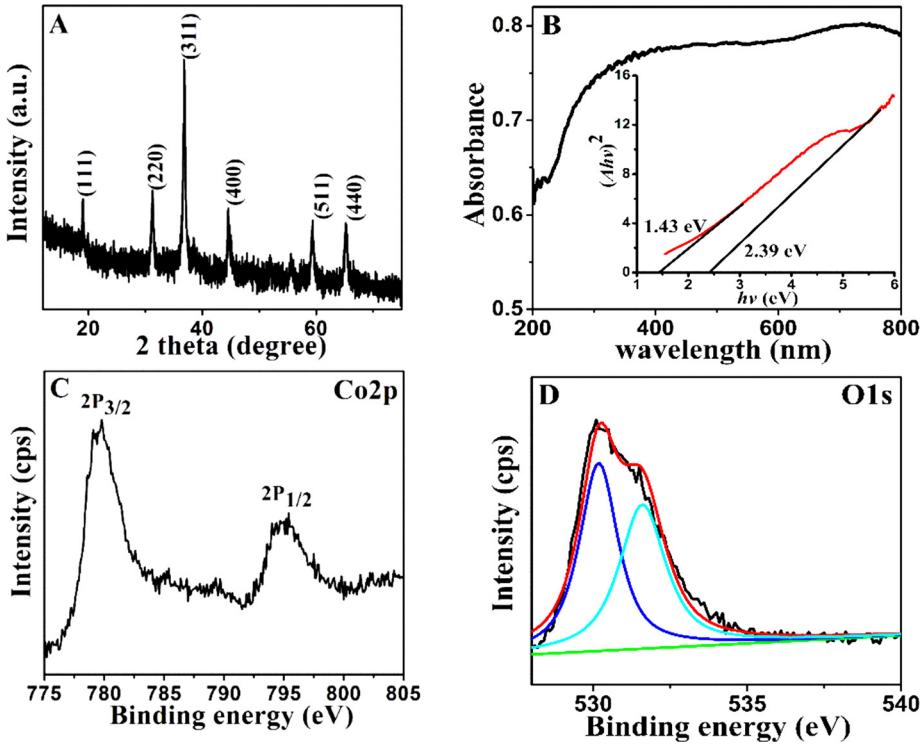

Fig. 1. (A) XRD patterns of Co_3O_4 nanorod arrays removed from Ni foam. (B) UV–vis diffuse reflectance spectra of Co_3O_4 nanorod-arrayed photocathode, with the inset of the corresponding plot of $(Ah\nu)^2$ versus $h\nu$. (C) Co 2p and (D) O 1s spectra of the Co_3O_4 nanorod-arrayed photocathode.

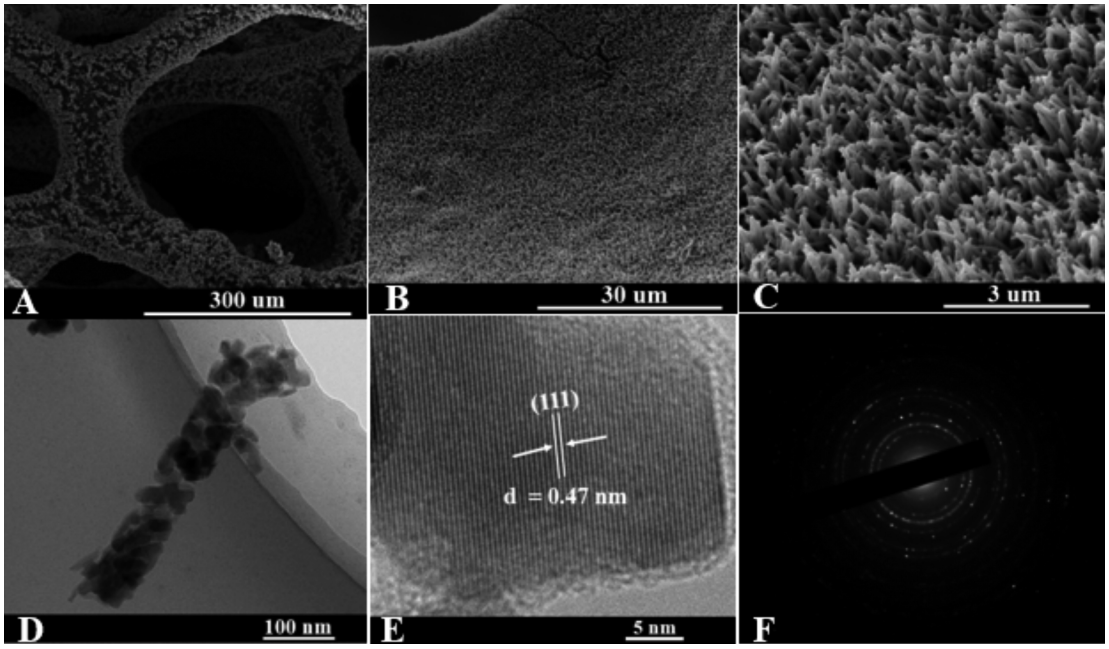

Fig. 2. (A) SEM image for the 3D hierarchical structure of the Co_3O_4 nanorod arrays growing on Ni foam. (B) Low-magnification SEM image of Co_3O_4 nanorod arrays viewed from the top. (C) Corresponding enlarged image of Co_3O_4 nanorod arrays viewed from the top. (D) TEM and (E) HRTEM images of a single Co_3O_4 nanorod and (F) corresponding SAED pattern.

(Fig. 5). The current density of the MPEC also showed stable and reproducible cycles over several on-off light irradiation cycles.

Polarization and power density curves were also obtained with and without light irradiation. The open circuit voltage under visible light was 608 ± 8 mV, compared to 571 ± 1 mV in the dark. The maximum power densities was 331 ± 4 mW m^{-2} with light irradiation, and 175 ± 25 mW m^{-2} without light (Fig. 6A). Based on the electrode potential curves (Fig. 6B), the anode potentials were the same under dark or light conditions, ranging from 0 to 0.98 A m^{-2} over a range of 0–1 A m^{-2}. However, the cathode potential was substantially improved with light, indicating the improved performance was due to the cathode.

3.4. Conversion of CO_2 into simple organic molecules

The catalytic activities for CO_2 conversion were examined (Fig. 7A).

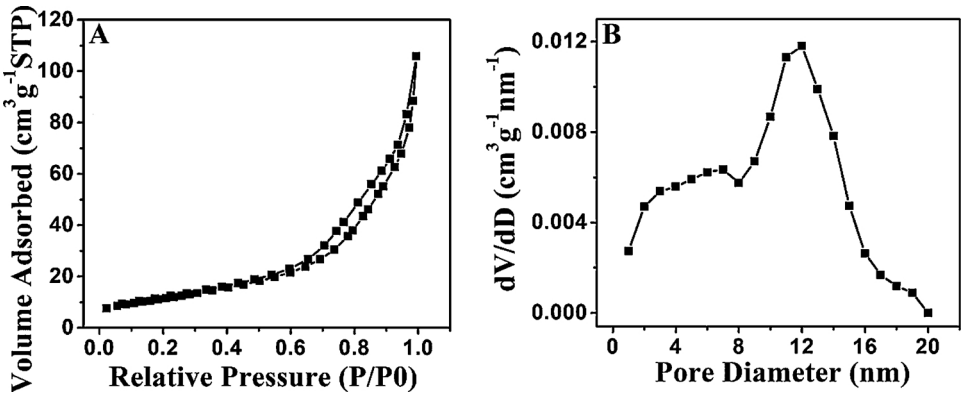

Fig. 3. (A) The N_2 adsorption-desorption isotherm loop. (B) The pore size distribution of the Co_3O_4 nanorod arrays scraped off from Ni foam.

For a single Co_3O_4 nanorod-arrayed photocathode in dark condition, no production was detected due to the absence of the electrons without irradiation. For the conditions of bare Co_3O_4 photocathode with light irradiation, the MPEC system with and without light irradiation, formic acid was the only product detected, indicating a high selectivity. The yield of formic acid produced by the single Co_3O_4 nanorod-arrayed photocathode under visible light irradiation was 133 ± 14 μmol through analysis of the catholyte after 10 h reaction. For the MPEC system with an external resistance of 300 Ω, the generation rate of formic acid was slow in the initial stage of CO_2 conversion, both under visible light and in dark, demonstrating that the anodic microorganisms needed time to adapt to this process. The yield of formic acid detected when the MPEC was operated under visible light irradiation in 10 h reaction time was 239 ± 10 μmol, which was about 4.9 times that produced by the MPEC operated in dark (49 ± 9 μmol), and 1.8 times that produced by a single Co_3O_4 nanorod-arrayed photocathode under visible light irradiation.

The COD removal efficiency in the anode of the MPEC system was 8.2 ± 0.9 % under visible light, which was 61 % larger than that obtained in dark (5.1 ± 0.4 %). The coulombic efficiency of the MPEC system was 10.5 ± 0.9 % under visible light, which was about 1.4 times that produced in dark (7.5 ± 1.2 %) (Fig. 7B). The enhanced catalytic activity for CO_2 conversion and improved coulombic efficiency were attributed to the Co_3O_4 photocathode, as the cathode potential was improved under light irradiation compared to the cathode in dark, while the anode potentials were essentially unchanged (Fig. 7C). The enhanced cathode potential under light irradiation made more electrons derived from the bio-anode driven to the photocathode through the external circuit, as shown by the higher current densities (Fig. 7D), leading to the enhanced coulombic efficiency and greatly improved separation of photogenerated electrons and holes of the

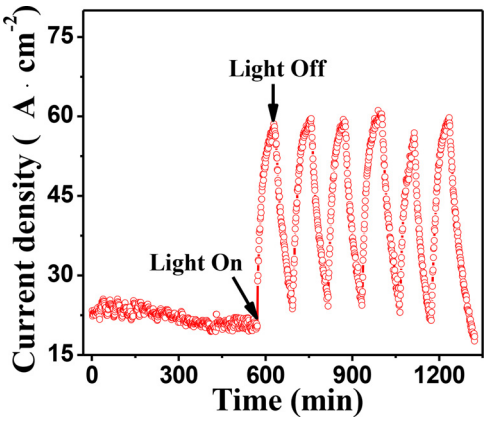

Fig. 5. Current density of the MPEC system with an external resistance of 300 Ω for several cycles of light on and off.

Co_3O_4 photocathode . Thus, the catalytic activity for CO_2 conversion to formic acid was also increased.

3.5. Discussion on the mechanism

A self-biased MPEC with a microbial anode and a Co_3O_4 nanorod-arrayed photocathode for spontaneous electricity generation and CO_2 reduction under visible light irradiation was successfully constructed, with the corresponding schematic diagram shown in Fig. 8. The reactions involved in the process of CO_2 reduction using this MPEC could be summarized as follows:

$$\text{Anode: } CH_3COO^- + 2H_2O \rightarrow 2CO_2 + 7H^+ + 8e^- \quad (1)$$

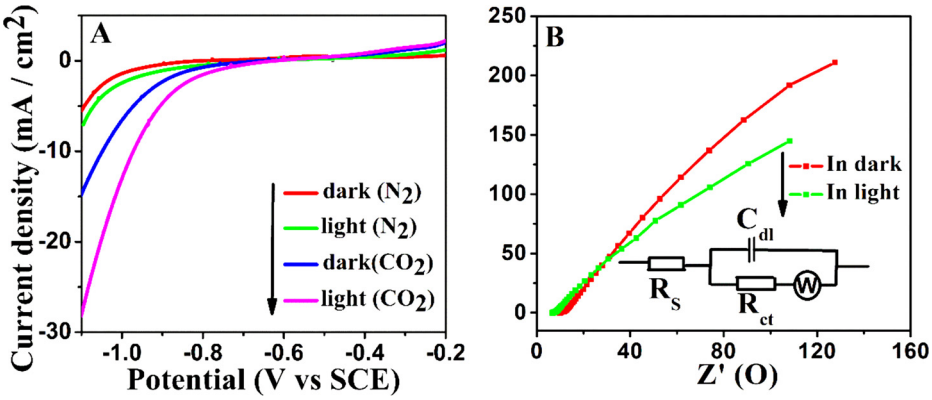

Fig. 4. (A) The linear sweep voltammetry curves of the Co_3O_4 nanorod-arrayed photocathode in 0.1 M Na_2SO_4 aqueous solution with N_2 or CO_2 saturated (B) Nyquist plots for electrochemical impedance spectra of the Co_3O_4 nanorod-arrayed photocathode under visible light and in dark (equivalent circuit in inset).

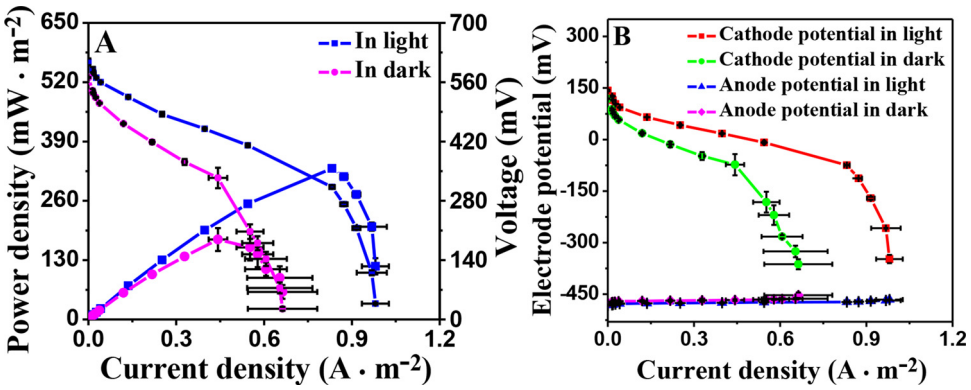

Fig. 6. Comparison of (A) polarization and power density (B) anode and cathode potentials curves of the MPEC system coupled with a Co_3O_4 nanorod-arrayed photocathode in light and in dark.

Cathode: $Co_3O_4 + h\nu \rightarrow h_{vb}^{+} + e_{cb}^{-}$ (2)

$e^{-} + h_{vb}^{+} \rightarrow h\nu$ (3)

$CO_2 + 2H^{+} + 2e_{cb}^{-} \rightarrow HCOOH$ (4)

In the anode of this MPEC, microorganisms degraded sodium acetate and produce electrical current, releasing protons into solution (reaction (1)). The electrons (e^{-}) derived from the bio-anode transferred to the photocathode continuously through the external circuit without external bias due to the higher potential of cathode than that of bio-anode. The protons and other cations were transferred to the cathode through the proton exchange membrane. In the cathode, when this MPEC was operated in the dark, Co_3O_4 functioned as an electrocatalyst and there was only a little formic acid detected in the cathode chamber (Fig. 7A). However, under visible light irradiation, photogenerated electrons (e_{cb}^{-}) and holes (h_{vb}^{+}) were generated on the conduction band and valence band of Co_3O_4 (reaction (2)), which improved the cathode potential and reduced the charge transfer resistance, as indicated in **Table S1** and Fig. 7**C**. Large amounts of photogenerated electron-hole pairs will recombine and only a fraction of electrons and holes could reach the surface of Co_3O_4 to take part in the chemical reactions. Thus, the separation of photogenerated electrons and holes is a key issue to influence the photocatalytic activity of Co_3O_4.

In this MPEC, the assistance of the electrons derived from bio-anode greatly enhanced the charge separation of Co_3O_4. Electrons produced by the bio-anode were driven to the photocathode through the external circuit because of the improved cathode potential and reduced cathode

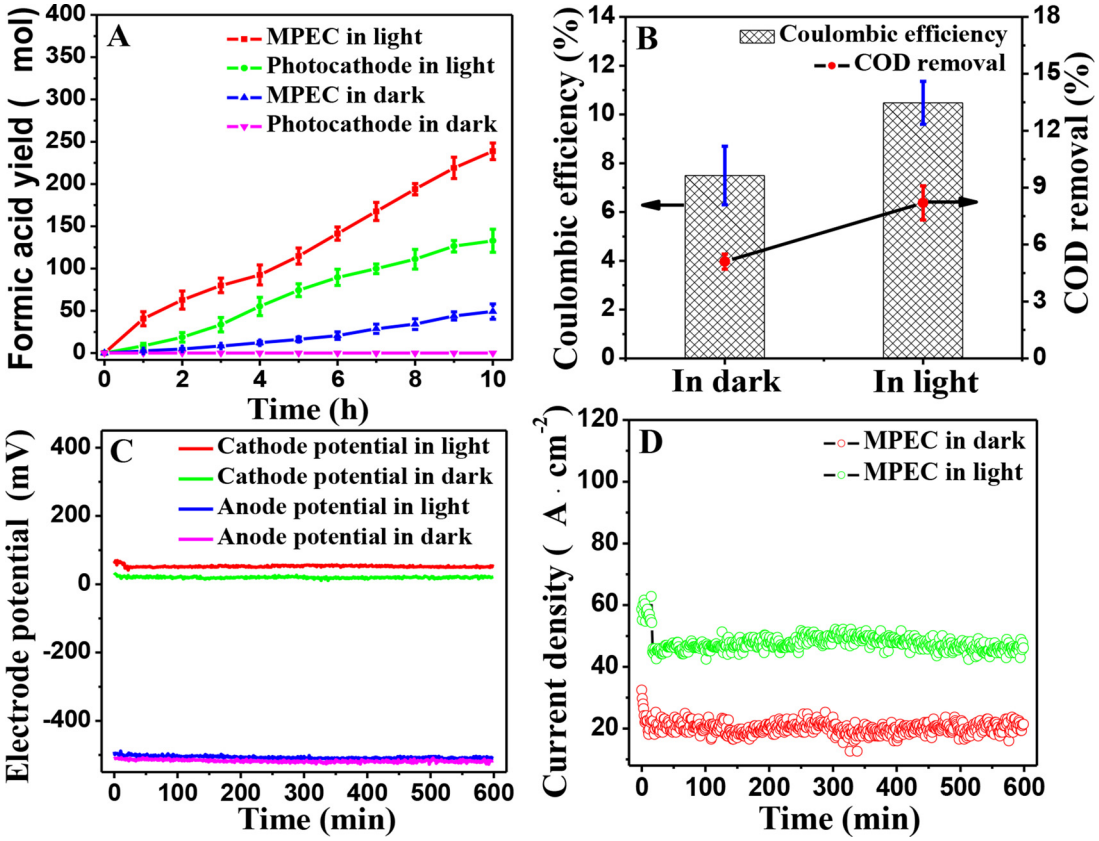

Fig. 7. (A) Catalytic activities for CO_2 conversion using a single Co_3O_4 nanorod-arrayed photocathode under visible light irradiation and in dark, MPEC system under visible light and in dark with an external resistance of 300 Ω. (B) COD removal and coulombic efficiencies (C) Electrode potentials (D) Current density of the MPEC system during the CO_2 conversion process under visible light irradiation and in dark with an external resistance of 300 Ω.

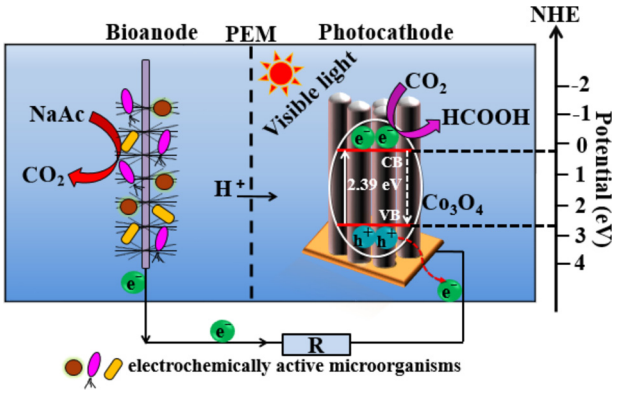

Fig. 8. Schematic of the charge-transfer process between a microbial anode and a Co_3O_4 nanorod-arrayed photocathode in an MPEC system under visible light irradiation.

charge transfer resistance caused by the photocatalysis of Co_3O_4. It is generally accepted that the energy potentials of electrons from the bio-anode were gradually lowered during the electron transfer process from the anode to cathode through the external circuit in an MPEC due to the electrolyte resistance, the resistance of electron transfer through the cellular respiratory chain, and electron transfer from microorganisms to anode. However, the energy potentials of the photogenerated electrons in cathode were higher than that of the electrons derived from bio-anode because of the absorption of light energy. Therefore, photo-generated holes on the valence band of Co_3O_4 preferentially combined with the electrons transferred from the anode, with the energy being released in the form of heat or photons (reaction (3)). As a result, the separation of photogenerated electrons and holes of Co_3O_4 was greatly improved, leading to an enhanced reaction kinetics of electrons and CO_2 reduction, and improved catalytic activity for CO_2 conversion to formic acid (reaction (4)), compared with the conditions of the single Co_3O_4 nanorod-arrayed photocathode for CO_2 reduction under visible light and the MPEC system in dark. Moreover, the enhanced reaction rate of CO_2 reduction could further enhance the power density of the MPEC. Thus, the photocathode and the bio-anode in this light sensitive MPEC system functioned synergistically coupled light energy and bioenergy for electricity generation and CO_2 conversion.

4. Conclusions

A microbial photoelectrochemical cell (MPEC) system using a bio-anode coupled with a Co_3O_4 nanorod-arrayed photocathode enabled efficient power generation and CO_2 conversion to formic acid. This MPEC system produced a maximal power density of 331 ± 4 mW m^{-2} under light irradiation, which was about 1.9 times of that produced in dark (175 ± 25 mW m^{-2}). With an external resistance of 300 Ω, 239 ± 10 μmol formic acid was obtained in the catholyte of this MPEC over a period of 10 h, which was 1.8 times of the formic acid produced by a bare Co_3O_4 nanorod-arrayed photocathode under visible light irradiation, and 4.9 times that produced by the MPEC operated in dark. The open circuit voltage of the MPEC system was improved to 608 ± 8 mV under light irradiation, which was 1.1 times of that in dark (571 ± 1 mV).

The enhanced CO_2 conversion performance and power density under light irradiation was due to the photocatalysis by the Co_3O_4 nanorod-arrayed photocathode, which improved the cathode potential and reduced the cathode charge transfer resistance. The activity of the photocathode allowed more electrons produced by the bio-anode to flow to the photocathode through the external circuit, enhancing the separation of photogenerated electrons and holes of Co_3O_4 and improving the reaction kinetics of electrons and CO_2 reduction. The MPEC therefore provides an efficient approach for simultaneous organic pollutant degradation and clean energy production due to the synergistic effect of combining bioenergy and light energy.

CRediT authorship contribution statement

Jing Wu: Investigation, Writing - original draft. **Xiaoyu Han:** Methodology. **Da Li:** Formal analysis. **B.E. Logan:** Writing - review & editing, Supervision. **Jia Liu:** Investigation. **Zhaohan Zhang:** Formal analysis. **Yujie Feng:** Supervision, Funding acquisition.

Declaration of Competing Interest

The authors declare that they have no known competing financial interests or personal relationships that could have appeared to influence the work reported in this paper.

Acknowledgements

This research work was financially supported by the National Key R &D Program of China (2017YFA0207201) and the National Natural Science Foundation of China (21673061 & 21972036). This work was also supported by the Open Project of State Key Laboratory of Urban Water Resource and Environment, Harbin Institute of Technology (No. QAK201534).

Appendix A. Supplementary data

Supplementary material related to this article can be found, in the online version, at doi:https://doi.org/10.1016/j.apcatb.2020.119102.

References

[1] M.B. Ross, P. De Luna, Y. Li, C.T. Dinh, D. Kim, P. Yang, E.H. Sargent, Designing materials for electrochemical carbon dioxide recycling, Nat. Catal. 2 (2019) 648–658.
[2] Y. Xu, Y. Jia, Y. Zhang, R. Nie, Z. Zhu, J. Wang, H. Jing, Photoelectrocatalytic reduction of CO_2 to methanol over the multi-functionalized TiO_2 photocathodes, Appl. Catal. B: Environ. 205 (2017) 254–261.
[3] P.R. Yaashikaa, P. Senthil Kumar, S.J. Varjani, A. Saravanan, A review on photochemical, biochemical and electrochemical transformation of CO_2 into value-added products, J. CO_2 Util 33 (2019) 131–147.
[4] J. Shi, Y. Jiang, Z. Jiang, X. Wang, X. Wang, S. Zhang, P. Han, C. Yang, Enzymatic conversion of carbon dioxide, Chem. Soc. Rev. 44 (2015) 5981–6000.
[5] X. Li, J. Yu, M. Jaroniec, X. Chen, Cocatalysts for selective photoreduction of CO_2 into solar fuels, Chem. Rev. 119 (2019) 3962–4179.
[6] X. Chang, T. Wang, J. Gong, CO_2 photo-reduction: insights into CO_2 activation and reaction on surfaces of photocatalysts, Energy Environ. Sci. 9 (2016) 2177–2196.
[7] J. Li, X. Zhang, F. Raziq, J. Wang, C. Liu, Y. Liu, J. Sun, R. Yan, B. Qu, C. Qin, L. Jing, Improved photocatalytic activities of g-C_3N_4 nanosheets by effectively trapping holes with halogen-induced surface polarization and 2,4-dichlorophenol decomposition mechanism, Appl. Catal. B: Environ. 218 (2017) 60–67.
[8] L. Wan, Q. Zhou, X. Wang, T.E. Wood, L. Wang, P.N. Duchesne, J. Guo, X. Yan, M. Xia, Y.F. Li, A.A. Jelle, U. Ulmer, J. Jia, T. Li, W. Sun, G.A. Ozin, Cu2O nanocubes with mixed oxidation-state facets for (photo)catalytic hydrogenation of carbon dioxide, Nat. Catal. 2 (2019) 889–898.
[9] J. Wu, D. Li, J. Liu, C. Li, Z. Li, B.E. Logan, Y. Feng, Enhanced charge separation of TiO_2 nanotubes photoelectrode for efficient conversion of CO_2, ACS Sustain. Chem. Eng. 6 (2018) 12953–12960.
[10] Y. Wang, Z. Wang, C.T. Dinh, J. Li, A. Ozden, M. Golam Kibria, A. Seifitokaldani, C.S. Tan, C.M. Gabardo, M. Luo, H. Zhou, F. Li, Y. Lum, C. McCallum, Y. Xu, M. Liu, A. Proppe, A. Johnston, P. Todorovic, T.T. Zhuang, D. Sinton, S.O. Kelley, E.H. Sargent, Catalyst synthesis under CO_2 electroreduction favours faceting and promotes renewable fuels electrosynthesis, Nat. Catal. (2019).
[11] D. Li, J. Wu, T. Liu, J. Liu, Z. Yan, L. Zhen, Y. Feng, Tuning the pore structure of porous tin foam electrodes for enhanced electrochemical reduction of carbon dioxide to formate, Chem. Eng. J. 375 (2019) 122024.
[12] D. Li, L. Huang, T. Liu, J. Liu, L. Zhen, J. Wu, Y. Feng, Electrochemical reduction of carbon dioxide to formate via nano-prism assembled CuO microspheres, Chemosphere. 237 (2019) 124527.
[13] J. Chen, C. Dong, H. Idriss, O.F. Mohammed, O.M. Bakr, Metal halide perovskites for solar-to-chemical fuel conversion, Adv. Energy Mater. (2019) 1902433.
[14] S.K. Kuk, Y. Ham, K. Gopinath, P. Boonmongkolras, Y. Lee, Y.W. Lee, S. Kondaveeti, C. Ahn, B. Shin, J.K. Lee, S. Jeon, C.B. Park, Continuous 3D titanium nitride nanoshell structure for solar-driven unbiased biocatalytic CO_2 reduction, Adv. Energy Mater. 9 (2019) 1900029.

[15] J.J. Leung, J. Warnan, K.H. Ly, N. Heidary, D.H. Nam, M.F. Kuehnel, E. Reisner, Solar-driven reduction of aqueous CO2 with a cobalt bis(terpyridine)-based photocathode, Nat. Catal. 2 (2019) 354–365.
[16] S. Xie, Q. Zhang, G. Liu, Y. Wang, Photocatalytic and photoelectrocatalytic reduction of CO_2 using heterogeneous catalysts with controlled nanostructures, Chem. Commun. 52 (2016) 35–59.
[17] Q. Shen, J. Ma, X. Huang, N. Yang, G. Zhao, Enhanced carbon dioxide conversion to formate on a multi-functional synergistic photoelectrocatalytic interface, Appl. Catal. B: Environ. 219 (2017) 45–52.
[18] E. Irtem, M.D. Hernández-Alonso, A. Parra, C. Fàbrega, G. Penelas-Pérez, J.R. Morante, T. Andreu, A photoelectrochemical flow cell design for the efficient CO_2 conversion to fuels, Electrochim. Acta 240 (2017) 225–230.
[19] J.Fd. Brito, M.V.B. Zanoni, On the application of Ti/TiO_2/CuO n-p junction semiconductor: a case study of electrolyte, temperature and potential influence on CO_2 reduction, Chem. Eng. J. 318 (2017) 264–271.
[20] P. Suyana, P. Ganguly, B.N. Nair, A.P. Mohamed, K.G.K. Warrier, U.S. Hareesh, Co_3O_4–C_3N_4 p–n nano-heterojunctions for the simultaneous degradation of a mixture of pollutants under solar irradiation, Environ. Sci. Nano 4 (2017) 212–221.
[21] G. Hu, C.X. Hu, Z.Y. Zhu, L. Zhang, Q. Wang, H.L. Zhang, Construction of Au/CuO/Co_3O_4 tricomponent heterojunction nanotubes for enhanced photocatalytic oxygen evolution under visible light irradiation, ACS Sustain. Chem. Eng. 6 (2018) 8801–8808.
[22] H.Q. Sun, H.M. Ang, M.O. Tadé, S.B. Wang, Co_3O_4 nanocrystals with predominantly exposed facets: synthesis, environmental and energy applications, J. Mater. Chem. A. 1 (2013) 14427–14442.
[23] Q. Shen, Z. Chen, X. Huang, M. Liu, G. Zhao, High-yield and selective photoelectrocatalytic reduction of CO_2 to formate by metallic copper decorated Co_3O_4 nanotube arrays, Environ. Sci. Technol. 49 (2015) 5828–5835.
[24] X. Huang, T. Cao, M. Liu, G. Zhao, Synergistic photoelectrochemical synthesis of formate from CO_2 on {121¯} Hierarchical Co_3O_4, J. Phys. Chem. C. 117 (2013) 26432–26440.
[25] X. Huang, Q. Shen, J. Liu, N. Yang, G. Zhao, A CO_2 adsorption-enhanced semiconductor/metal-complex hybrid photoelectrocatalytic interface for efficient formate production, Energy Environ. Sci. 9 (2016) 3161–3171.
[26] B. Min, B.E. Logan, Continuous electricity generation from domestic wastewater and organic substrates in a flat plate microbial fuel cell, Environ. Sci. Technol. 38 (2004) 5809–5814.
[27] H. Liu, B.E. Logan, Electricity generation using an air-cathode single chamber microbial fuel cell in the presence and absence of a proton exchange membrane, Environ. Sci. Technol. 38 (2004) 4040–4046.
[28] B.E. Logan, J.M. Regan, Microbial fuel cells: challenges and applications, Environ. Sci. Technol. 40 (2006) 5172–5180.
[29] F. Qian, G. Wang, Y. Li, Solar-driven microbial photoelectrochemical cells with a nanowire photocathode, Nano Lett. 10 (2010) 4686–4691.
[30] Z. Sun, R. Cao, M. Huang, D. Chen, W. Zheng, L. Lin, Effect of light irradiation on the photoelectricity performance of microbial fuel cell with a copper oxide nanowire photocathode, J. Photochem. Photobiol. A. 300 (2015) 38–43.
[31] D. Liang, G. Han, Y. Zhang, S. Rao, S. Lu, H. Wang, Y. Xiang, Efficient H_2 production in a microbial photoelectrochemical cell with a composite Cu_2O/NiO_x photocathode under visible light, Acs Appl. Energy Mater. 168 (2016) 544–549.
[32] H. Dong, H. Yu, X. Wang, Q. Zhou, J. Feng, A novel structure of scalable air-cathode without nafion and Pt by rolling activated carbon and PTFE as catalyst layer in microbial fuel cells, Water Res. 46 (2012) 5777–5787.
[33] B.E. Logan, E. Zikmund, W. Yang, R. Rossi, K.Y. Kim, P.E. Saikaly, F. Zhang, Impact of ohmic resistance on measured electrode potentials and maximum power production in microbial fuel cells, Environ. Sci. Technol. 52 (2018) 8977–8985.
[34] B.P. Cario, R. Rossi, K.Y. Kim, B.E. Logan, Applying the electrode potential slope method as a tool to quantitatively evaluate the performance of individual microbial electrolysis cell components, Bioresour. Technol. 287 (2019) 121418.
[35] S. Cheng, H. Liu, B.E. Logan, Increased performance of single-chamber microbial fuel cells using an improved cathode structure, Electrochem. commun. 8 (2006) 489–494.
[36] D. Barreca, C. Massignan, S. Daolio, M. Fabrizio, C. Piccirillo, L. Armelao, E. Tondello, Composition and microstructure of cobalt oxide thin films obtained from a novel cobalt(II) precursor by chemical vapor deposition, Chem. Mater. 13 (2001) 588–593.
[37] Y. Shang, X. Chen, W. Liu, P. Tan, H. Chen, L. Wu, C. Ma, X. Xiong, J. Pan, Photocorrosion inhibition and high-efficiency photoactivity of porous g-C_3N_4/Ag_2CrO_4 composites by simple microemulsion-assisted co-precipitation method, Appl. Catal. B: Environ. 204 (2017) 78–88.
[38] H. Cao, Y. Lu, W. Ning, H. Zhang, G. Zheng, Co_3O_4 nanoparticles modified TiO_2 nanotube arrays with improved photoelectrochemical performance, Russ. J. Appl. Chem. 92 (2019) 64–70.
[39] E.M. Ngigi, P.N. Nomngongo, J.C. Ngila, Novel Z-scheme Co_3O_4/WO_3 nanocomposite performance in adsorption and photocatalytic degradation of ethylparaben and methylene blue in water, Adv. Nat. Sci.: Nanosci. Nanotechnol. 10 (2019) 045018.
[40] C. Yuan, L. Yang, L. Hou, L. Shen, X. Zhang, X.W. Lou, Growth of ultrathin mesoporous Co_3O_4 nanosheet arrays on Ni foam for high-performance electrochemical capacitors, Energy Environ. Sci. 5 (2012) 7883.
[41] L. Wang, S. Zhang, Y. Zhu, A. Patlolla, J. Shan, H. Yoshida, S. Takeda, A.I. Frenkel, F. Tao, Catalysis and in situ studies of Rh1/$Co3O_4$ nanorods in reduction of NO with H_2, ACS Catal. 3 (2013) 1011–1019.
[42] C. Yuan, L. Yang, L. Hou, L. Shen, F. Zhang, D. Li, X. Zhang, Large-scale Co_3O_4 nanoparticles growing on nickel sheets via a one-step strategy and their ultra-highly reversible redox reaction toward supercapacitors, J. Mater. Chem. 21 (2011) 18183–18185.
[43] J. Zhang, W. Gao, M. Dou, F. Wang, J. Liu, Z. Li, J. Ji, Nanorod-constructed porous Co_3O_4 nanowires: highly sensitive sensors for the detection of hydrazine, Analyst 140 (2015) 1686–1692.
[44] F. Zhang, C. Yuan, X. Lu, L. Zhang, Q. Che, X. Zhang, Facile growth of mesoporous Co_3O_4 nanowire arrays on Ni foam for high performance electrochemical capacitors, J. Power Sources 203 (2012) 250–256.